Continental Shelf Research 64 (2013) 51–65

Contents lists available at SciVerse ScienceDirect

Continental Shelf Research

journal homepage: www.elsevier.com/locate/csr

Research papers

Numerical study of the sensitivity of mangroves in reducing storm surge and flooding to hurricane characteristics in southern Florida

Huiqing Liu [a,*], Keqi Zhang [a], Yuepeng Li [a], Lian Xie [b]

[a] International Hurricane Research Center, Florida International University, MARC 370, Miami, FL 33199, United States
[b] Department of Marine, Earth and Atmospheric Sciences, North Carolina State University, Box 8208, Raleigh, NC 27695, United States

ARTICLE INFO

Article history:
Received 21 March 2013
Received in revised form
28 May 2013
Accepted 30 May 2013
Available online 10 June 2013

Keywords:
Mangroves
Storm surge
Hurricane
Surge attenuation
Storm surge modeling

ABSTRACT

The sensitivity of the mangrove effect on reducing storm surge flooding to hurricane characteristics is investigated by using the numerical model Coastal and Estuarine Storm Tide (CEST). First, the attenuation of storm surge by mangroves is incorporated into the model by updating Manning's coefficient based on the National Land Cover Dataset (NLCD) 2001. Then CEST is verified by comparing the model results with field observations in South Florida for Hurricane Wilma. Secondly, a set of numerical experiments using synthetic hurricanes with different intensity, forward speed, radius of maximum wind speed and travel direction are conducted for the sensitivity study. Results indicate that storm surge magnitudes and flooding areas are reduced by the mangrove zone more for fast moving hurricanes than slow moving hurricanes in the west coast of South Florida. In addition, increasing hurricane intensity and hurricane size lower the effect of mangroves on attenuating storm surge and reducing the flooding area. The mangrove zone plays a more effective role in reducing flooding areas from hurricanes that travel from east to west than from hurricanes that travel from west to east. The mangrove reduction effect is most sensitive to changes in hurricane forward speed. A 6.7 m/s to 2.2 m/s decrease in forward speed can result in a decrease in flood area reduction by mangroves that is equivalent to the decrease in flood area reduction by mangroves from Category 3 to 5 hurricanes.

1. Introduction

A storm surge is an abnormal rise of the water surface in an ocean or lake associated with a low pressure weather system, typically a hurricane. Storm surge and associated flooding often lead to loss of human life, and destruction of property and infrastructure in populated, low-lying coastal areas. For example, Hurricane Katrina struck southern Louisiana and Mississippi in 2005, causing at least 1836 people to lose their lives, making it one of the deadliest United States hurricanes. Hurricane Hugo made landfall in Charleston, South Carolina in 1989, resulting in $5 billion damage in South Carolina.

Numerical models play an important role in reducing the property damage and loss of life caused by storm surges. Many storm surge models have been developed since the advent of the computer in the 1960s. For example, the Sea, Lake, and Overland Surge from Hurricane (SLOSH) model on a conformal grid was developed by the National Weather Service (NWS) of the National Oceanic and Atmospheric Administration (NOAA) (Jelesnianski et al., 1992). Public announcements and evacuation decisions from federal and state agencies before hurricane landfall have been based on the results of the SLOSH model. SLOSH has made an important contribution to reducing fatalities and property loss over the last several decades, but it has several limitations due to the utilization of linearized equations and algorithms. The Coastal and Estuarine Storm Tide (CEST) model for a curvilinear grid overcomes these limitations by including nonlinear items in momentum equations and using a semi-implicit discrete scheme (Zhang et al., 2008a). Zhang et al. (2008a) showed the storm surge simulation was improved by CEST through a detailed comparison of the CEST and SLOSH results to field measurements from historical hurricanes. In order to better resolve coastal complex geomorphic features such as rivers, canals, and barrier islands, unstructured-grid, finite-element numerical models such as FVCOM (Chen et al., 2003) and ADCIRC (Westerink et al., 1992) have been developed. These models have been validated by using several historical hurricanes in different areas and showed good agreements with field observations (Westerink et al., 2008; Mattocks and Forbes, 2008; Weisberg and Zheng, 2006).

In addition to a better representation of hydrologic and geomorphic features in a model domain using various grid structures, many physical processes such as wind waves, tides and river discharge have been added to storm surge models to improve model performance. Xie et al. (2008) and Liu and Xie

* Corresponding author. Tel.: +1 305 348 1607.
E-mail address: huliu@fiu.edu (H. Liu).

0278-4343/$ - see front matter © 2013 Elsevier Ltd. All rights reserved.
http://dx.doi.org/10.1016/j.csr.2013.05.015

(2009) developed a wave–surge coupled model, and their results showed that wave–surge coupled models could improve the storm surge, flooding and wave forecast. Rego and Li (2010) indicated that incorporating nonlinear tide effects into storm surge models could cause noticeably different results compared to adding the tides linearly. Westerink et al. (2008) coupled the ADCIRC model with tides and river flow, and the model validation through Hurricanes Betsy and Andrew showed a good performance.

In spite of these improvements in modeling storm surge, many models suffer a common drawback, neglecting the effect of coastal land cover on overland flooding by using a constant bottom friction coefficient. Physically, different land cover types such as forest and bare land have different effects on wind stress and bottom friction force. As a result, the surge inundation process in the vegetated area should differ from that in the bare land area. Westerink et al. (2008) incorporated the effects of land cover on bottom friction and surface wind into the ADCIRC model. The application of the ADCIRC model to investigating the wetland effect on storm surges along the Louisiana coast showed that the attenuation rate of the wetland on storm surges is not a constant and depends on many factors such as the storm's track, size, the regional bathymetry and topography (Resio and Westerink, 2008). The studies by Loder et al. (2009) and Wamsley et al. (2009) showed that coastal wetlands offer protection from storm surge and waves. The further investigation of Wamsley et al. (2010) suggested that wetlands do have the potential to reduce surges, but that it depends on the surrounding coastal landscape and the strength and duration of a storm.

Mangroves are one of the main types of forest growing in tropical and subtropical coastal areas. The mangrove community has been valued for its protection of uplands from wind, wave, and flood impacts; however, few studies on mangrove effects on inundation have been conducted (McIvor et al., 2012a, 2012b). Yanagisawa et al. (2010) studied the performance of mangroves in reducing damage from the 2004 Indian Ocean tsunami. Sheng et al. (2012) simulated the reduction of storm surge by vegetation canopies by using idealized topographies covered by different vegetation canopies. They found that the effectiveness of the vegetation in dissipating storm surge and inundation depends on different storms and canopy parameters. However, their results have not been verified by field observations. Zhang et al. (2012) investigated the role of mangroves in attenuating storm surge using Hurricane Wilma. They found that the mangrove forest could provide effective protection of inlands by attenuating storm surge from Hurricane Wilma (Category 3), but could not be able to attenuate storm surge completely from a slowly moving Category 5 hurricane. Zhang et al.'s study only considered Hurricane Wilma and synthetic Category 5 hurricanes following the same path of Wilma. The variation of hurricane parameters on mangrove attenuation effects has not been investigated thoroughly. The purpose of this paper is to extend the study of Zhang et al. (2012) to explore the sensitivity of mangrove effects in reducing storm surge and flooding to sets of synthetic hurricanes with different intensity, forward speed, radius of maximum wind speed and various track directions.

The rest of the manuscript is organized as follows: the CEST model is briefly described in Section 2. Section 3 introduces the details of how to incorporate the land cover data into the CEST model. The validation of the model is presented in Section 4. The settings and results of sensitivity numerical experiments are provided in Section 5. The summary and conclusion are given in Section 6.

2. CEST model

The CEST model is a two-dimensional, finite difference model developed by Zhang et al. (2008a) to simulate estuarine and coastal flooding induced by hurricanes. The CEST model is forced by winds, atmospheric pressures, and astronomical tides or a time series of water levels at open boundaries. It is capable of simulating storm tides as well as the wind-driven circulation at estuaries and coasts.

The governing equations in Cartesian coordinate are

$$\frac{\partial u'}{\partial x}+\frac{\partial v'}{\partial y}+\frac{\partial w'}{\partial z}=0 \tag{2-1}$$

$$\frac{\partial u'}{\partial t}+u'\frac{\partial u'}{\partial x}+v'\frac{\partial u'}{\partial y}+w'\frac{\partial u'}{\partial z}-fv'=\frac{\partial}{\partial z}\left[A_v\frac{\partial u'}{\partial z}\right]-\frac{1}{\rho_o}\frac{\partial P}{\partial x}+\frac{\partial}{\partial x}\left(2A_h\frac{\partial u'}{\partial x}\right)+\frac{\partial}{\partial y}\left(A_h\left(\frac{\partial u'}{\partial y}+\frac{\partial v'}{\partial x}\right)\right) \tag{2-2}$$

$$\frac{\partial v'}{\partial t}+u'\frac{\partial v'}{\partial x}+v'\frac{\partial v'}{\partial y}+w'\frac{\partial v'}{\partial z}+fu'=\frac{\partial}{\partial z}\left[A_v\frac{\partial v'}{\partial z}\right]-\frac{1}{\rho_o}\frac{\partial P}{\partial y}+\frac{\partial}{\partial y}\left(2A_h\frac{\partial v'}{\partial y}\right)+\frac{\partial}{\partial y}\left(A_h\left(\frac{\partial u'}{\partial y}+\frac{\partial v'}{\partial x}\right)\right) \tag{2-3}$$

$$\rho g=-\frac{\partial P}{\partial z} \tag{2-4}$$

where t is time, u', v', and w' are the eastward, northward, and vertical Cartesian velocities, ρ_o is the reference density, ρ is the in situ density, g is the gravitational acceleration, P is the pressure, A_v is the vertical eddy diffusivity, A_h is the horizontal eddy diffusivity, and f is the Coriolis parameter.

By integrating the above equations over the depth from the bottom $z=H$ to surface $z=-\zeta$, an equation for the surface elevation can be written as

$$\frac{\partial \zeta}{\partial t}+\frac{\partial HU}{\partial x}+\frac{\partial HV}{\partial y}=0 \tag{2-5}$$

$$\frac{\partial HU}{\partial t}+\frac{\partial HU^2}{\partial x}+\frac{\partial HUV}{\partial y}=fHV-g\frac{\partial}{\partial x}\left(\zeta+\frac{\Delta P_a}{\rho g}\right)-\frac{\tau_B^x}{\rho_0}+\frac{\tau_T^x}{\rho_0}+A_h\frac{\partial^2 HU}{\partial x^2}+A_h\frac{\partial^2 HU}{\partial y^2} \tag{2-6}$$

$$\frac{\partial HV}{\partial t}+\frac{\partial HUV}{\partial x}+\frac{\partial HV^2}{\partial y}=-fHU-g\frac{\partial}{\partial y}\left(\zeta+\frac{\Delta P_a}{\rho g}\right)-\frac{\tau_B^y}{\rho_0}+\frac{\tau_T^y}{\rho_0}+A_h\frac{\partial^2 HV}{\partial x^2}+A_h\frac{\partial^2 HV}{\partial y^2} \tag{2-7}$$

where U and V are vertically integrated velocities

$$(U,\ V)=\int_H^{-\zeta}(u',v')\,dz$$

ΔP_a is the air pressure drop.

The bottom friction is written as

$$\tau_B^x=\rho_0 C_B\sqrt{U^2+V^2}U \tag{2-8}$$

$$\tau_B^y=\rho_0 C_B\sqrt{U^2+V^2}V \tag{2-9}$$

C_B is bottom friction coefficient, which is calculated by

$$C_B=\frac{gn^2}{H^{1/3}} \tag{2-10}$$

where n is Manning's coefficient and H is the total water depth. The same principle is used to describe the air–water interface. Any law of wind friction for τ_T^x which can be written in the form

$$\tau_T^x=\rho_a C_d\sqrt{(U_a-U)^2+(V_a-V)^2}(U_a-U) \tag{2-11}$$

$$\tau_T^y=\rho_a C_d\sqrt{(U_a-U)^2+(V_a-V)^2}(V_a-V) \tag{2-12}$$

where C_d is the surface wind drag coefficient, which was calculated by modified Large and Pond (1981) formula.

$$C_d = \begin{cases} 0.00114 & \sqrt{U_a^2 + V_a^2} \le 10 \\ \left(0.49 + 0.065\sqrt{U_a^2 + V_a^2}\right)0.001 & 10 < \sqrt{U_a^2 + V_a^2} \le 38 \\ 0.003 & \sqrt{U_a^2 + V_a^2} > 38 \end{cases} \quad (2-13)$$

U_a and V_a are the 10 m height wind velocities along the x and y directions.

3. Calculation of Manning's coefficient values based on land cover data

Incorporating land cover data into the storm surge and flooding model is necessary for overland flooding simulation because it modulates the water flow velocity through influencing the wind stress and bottom friction force. The parametric wind model used by SLOSH (Jelesnianski et al., 1992) is employed to compute the hurricane wind field forcing CEST. To account for the land cover effect on the wind stress, first, two different drag coefficients in the SLOSH parametric wind model are used to compute the wind field on the terrain and extreme shallow waters and the wind field on the ocean. Then, the wind speed on the vegetated area is further adjusted using a coefficient C_T based on the ratio of the surge water depth ($D=H+\zeta$) to the vegetation height (H_T):

$$C_T = \begin{cases} \frac{D}{H_T} & D < H_T \\ 1 & D \ge H_T \end{cases} \quad (3-1)$$

The land cover effect on bottom friction is parameterized by calculating Manning's coefficient in Eq. (2-10) based on land cover types and coverage from the 2001 National Land Cover Dataset (NLCD) with a spatial resolution of 30 m (Homer et al., 2004). Manning's coefficient values for each land cover class used in this study are shown in Table 1 (modified from Mattocks and Forbes (2008)), in which mangroves are classified as Woody Wetlands class (i.e. Manning's coefficient=0.14). Based on the previous studies (Xu et al., 2010; Zhang et al., 2012), Manning's coefficient in the class of Woody Wetlands was changed from 0.1 to 0.14 because mangrove trees are denser than regular trees. Since the pixel size of the NLCD data set is typically smaller than the cell size of the model grid, an average Manning's coefficient (n_a) for a grid cell is calculated using all pixels within the cell by

$$n_a = \frac{\sum_{i=1}^{N}(n_i a) + n_0\beta}{Na + \beta} \quad (3-2)$$

where n_i are Manning's coefficient values of a NLCD pixel within a model grid cell, α is the area of a NLCD pixel, N is the total number of NLCD pixels within a model cell, n_0 is constant Manning's coefficient, 0.02, for the area, β, that are not covered by NLCD pixels. Since NLCD data covers all land areas in the North America, Manning's coefficients for the land cells in the model domain are computed solely using NLCD pixel values and the value of β is zero. Only the calculation of Manning's coefficients for the grid cells covering both land and ocean areas involve non-zero β values.

The details of calculating Manning's coefficient value based on NLCD can be found in Zhang et al. (2012). The calculated Manning's coefficient values of the model basin are shown in Fig. 1.

Table 1
NCLD land cover classes with assigned values for the Manning's friction coefficient.

NLCD class number	NLCD class name	Manning's n friction coefficient
11	Open water	0.020
12	Perennial ice/snow	0.010
21	Developed open space	0.020
22	Developed low intensity	0.050
23	Developed medium intensity	0.100
24	Developed high intensity	0.130
31	Barren land (rock/sand/clay)	0.090
32	Unconsolidated shore	0.040
41	Deciduous forest	0.100
42	Evergreen forest	0.110
43	Mixed forest	0.100
51	Dwarf scrub	0.040
52	Shrub/scrub	0.050
71	Grassland/herbaceous	0.034
72	Sedge/herbaceous	0.030
73	Lichens	0.027
74	Moss	0.025
81	Pasture/hay	0.033
82	Cultivated crops	0.037
90	Woody wetlands	0.140
91	Palustrine forested wetland	0.100
92	Palustrine scrub/shrub wetland	0.048
93	Estuarine forested wetland	0.100
94	Estuarine scrub/shrub wetland	0.048
95	Emergent herbaceous wetlands	0.045
96	Palustrine emergent wetland (persistent)	0.045
97	Estuarine emergent wetland	0.045
98	Palustrine aquatic bed	0.015
99	Estuarine aquatic bed	0.015

4. Hurricane Wilma experiment

4.1. Experiments

Before the CEST model is applied to conduct a sensitivity analysis to investigate the effects of the mangrove zone on storm surge and overland flooding, the CEST model is validated with observed data from Hurricane Wilma. Wilma made landfall at the western coast of Florida in 2005, providing an ideal case to validate modeling storm surges across the mangrove zone as shown by the best track in Fig. 1.

4.2. Model settings

Fig. 1 shows the domain used by the CEST model for Hurricane Wilma. The grid includes both the east and west parts of Florida extending from 83.4°W to 78.7°W in longitude and from 27.2°N to 24.2°N in latitude, which can simulate hurricane induced storm surges along both Atlantic and Gulf coasts of South Florida. In addition, instead of following a straight line, the inland boundary of the grid fits curved linear features with higher elevations such as coastal ridges so their effect on blocking storm surges can be simulated. The grid resolution is about 240–300 m around the landfall area, about 1250–1550 m in the open ocean.

The 30×30 m U.S. Geological Survey (USGS), 8×8 m light detection and ranging, and 30×30 m airborne height finder DEMs data (Zhang et al., 2012) are used to derive the elevation over the land cells grid if the data are available for the study area. The NOAA 1-min Global Relief Model (ETOPO1) and 3-arcsecond Coastal Relief Model are combined to obtain bathymetric data for the water cells.

The tidal component is excluded from the simulation because of a small tidal range (0.3–0.6 m) in the study area (He and Weisberg, 2002). The partial clamped gravity wave radiation open boundary equation (Blumberg and Kantha, 1983) is used to define the water elevation at a lateral open boundary:

$$\frac{\partial \zeta}{\partial t} + C_0 \frac{\partial \zeta}{\partial n} = -\frac{(\zeta - \zeta_k)}{T_f} \quad (4-1)$$

where $C_0=(gH)^{1/2}$ is the phase speed of waves and n is the direction normal to the planar boundary. ζ_k is the known water

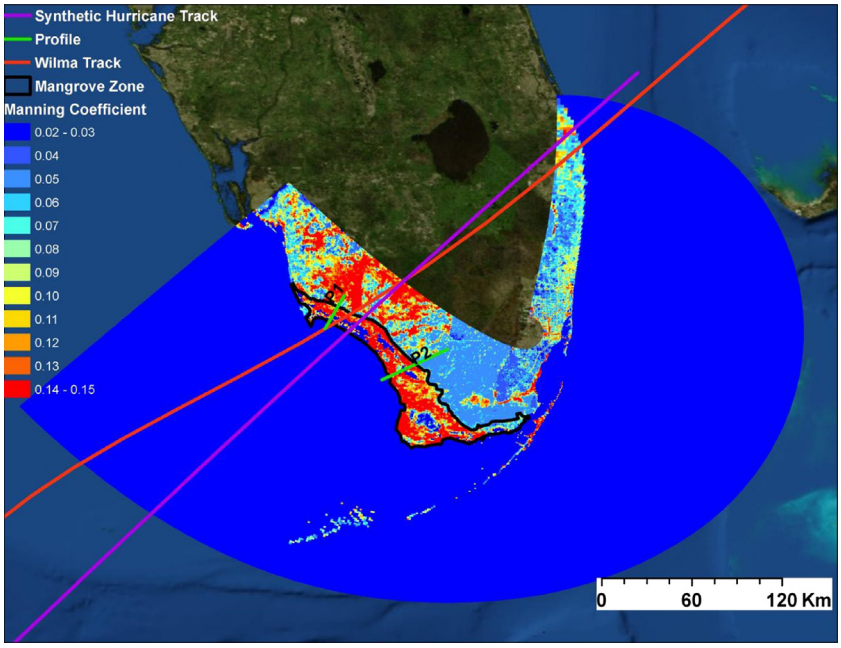

Fig. 1. Southern Florida Domain of CEST model, calculated Manning's coefficient based on National Land Cover Dataset (NLCD) 2001, the location of mangrove zone in the southern Florida domain, two profile lines passing through mangrove zone to sample the maximum storm surge height, and the best track of Hurricane Wilma and the track of synthetic hurricanes overlayed on the domain.

level value and T_f=the damping time scale, the value of which is different in different basins.

The parametric hurricane wind field model used by SLOSH (Jelesnianski et al., 1992) is used to generate Hurricane Wilma. The governing equations of the hurricane wind model are

$$\frac{1}{\rho}\frac{dp}{dr} = \frac{k_s V^2}{\sin\ \phi} - V\frac{dV}{dr} \qquad (4-2)$$

$$\frac{1}{\rho}\frac{dp}{dr}\cos\ \phi = fV + \frac{V^2}{r}\cos\ \phi - V^2\frac{d\phi}{dr}\sin\ \phi + k_n V^2 \qquad (4-3)$$

$$V(r) = V_R\frac{2Rr}{R^2 + r^2} \qquad (4-4)$$

where r is the distance from the storm center, V is the wind speed, ϕ is the inflow angle across circular isobars toward the storm center, V_R is the maximum wind, R is the radius for maximum wind speed, k_s and k_n are the empirically determined coefficients, and f is the Coriolis force coefficient.

4.3. Results

Fig. 2 shows the modeled peak storm surge height distribution induced by Hurricane Wilma for the whole domain. Storm surge reaches its peak values near the Wilma landfall coastal area. The time series of storm surge from the model simulation and observed data at 4 NOAA stations, which are indicated in Fig. 2, are shown in Fig. 3. The tide effects are removed from recorded data and both of the model results and observed data are adjusted to the NAVD88 vertical datum. The root mean square errors in those stations are 0.27, 0.16, 0.20 and 0.13 m. The time phases to reach peak surges are almost the same at the last three stations. There is a 4 h shift to reach the peak surge between the CEST model results and observation data in the first station (Naples). This result indicates that the CEST model performs well at simulating Wilma's storm surge at water areas. The comparison between modeled and observed peak storm surge from USGS at overland stations shows that the root mean square error is 0.39 m, indicating that the CEST model not only simulated surge well in water areas, but also captured storm surge successfully after water flows onto land. The detailed validation of the model can be found in the study of Zhang et al. (2012).

5. Sensitivity numerical experiments

5.1. Experiments

In order to investigate the sensitivity of effects of mangroves on storm surge to different hurricane characteristics (i.e. forward speed, intensity, maximum wind speed radius, hurricane moving direction), 18 synthetic hurricanes with different categories (3, 4 and 5 on the Saffir–Simpson scale with center pressure 953, 933 and 913 hPa respectively), forward speeds (2.2, 6.7 and 11.2 m/s or 5, 15 and 25 mph) and radius of maximum wind speed (32 and 56 km or 20 and 35 mile), and another nine category 3 synthetic hurricanes with same forward speeds (6.7 m/s or 15 mph), radius of maximum wind speed (32.2 km or 20 mile), same landfall location but with 9 different track moving directions, are employed to conduct storm surge simulations. Table 2-1 shows the settings of experiment group A composing 6 synthetic category 3 (center pressure 953 hPa) hurricanes; the settings of 6 synthetic category 4 (center pressure 933 hPa) hurricanes are shown in Table 2-2 named experiment group B; and the settings of 6 synthetic category 5 (center pressure 913 hPa) hurricanes are shown in Table 2-3 named experiment group C. Nine category 3 hurricanes with different moving directions (from 0° to 180°) are shown in Table 2-4, which are included in experiment group D. Based on historical hurricane records for the North Atlantic basin from 1851 to 2006, these nine different moving directions cover most possible tracks of major hurricanes (category 2 and up) influencing the mangrove zone in western Florida areas (Zhang et al., 2008b). In this study, the hurricane moving direction (approach angle) is defined as the angle (measured clockwise) in degrees between x direction (east horizontal line) and the hurricane moving track, e.g. 0° means hurricane moves from east to west horizontally (Fig. 4). All the hurricanes in experiments A, B and C have the same track (similar to Hurricane Wilma's track) and landfalling time except the length of track

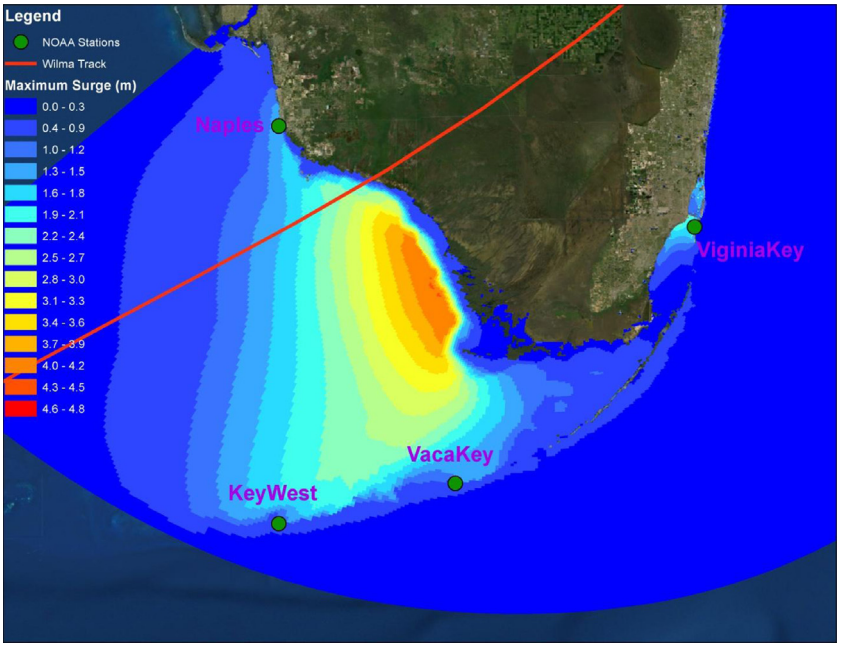

Fig. 2. The simulated maximum storm surge distribution during Hurricane Wilma, and the locations of 4 NOAA stations (Naples, KeyWest, VacaKey and ViginiaKey).

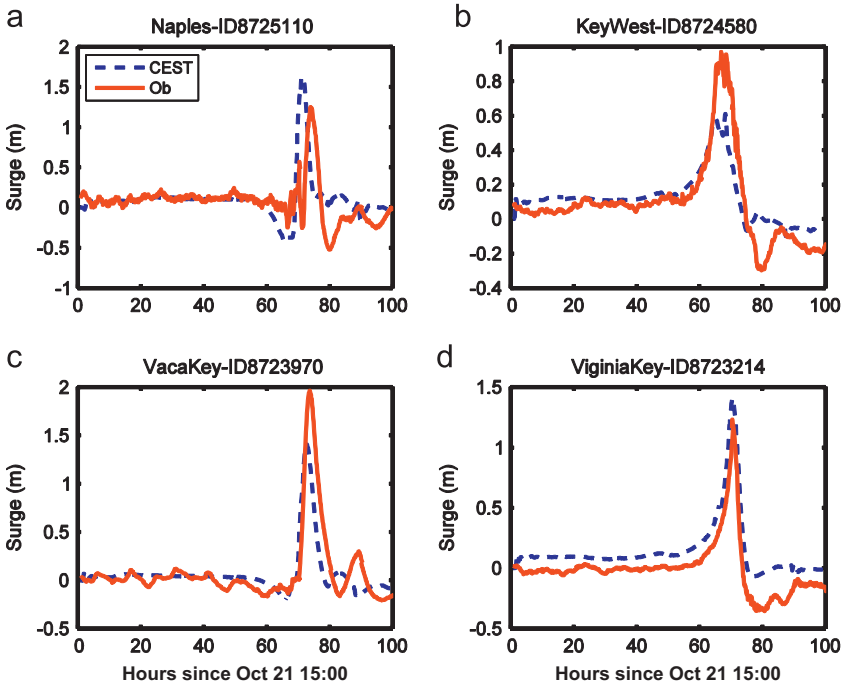

Fig. 3. Time series of storm surge during Hurricane Wilma (100 h since UTM 15:00 of October 21) at NOAA stations (a) Naples, (b) KeyWest, (c) VacKey, and (d) ViginiaKey. Solid line is oberved data and dashed line is CEST model results.

(slower moving hurricane has shorter track within the same time range), which is shown in Fig. 1. Fig. 4 shows the tracks of 9 hurricanes with different moving directions and shows the definition of the approach angle. All of the synthetic hurricanes data is provided by the National Hurricane Center.

5.2. Model settings

The same CEST domain, boundary condition and wind field model as that used for Hurricane Wilma are used in the numerical experiments. To evaluate the effects of mangroves on storm surge, two model settings are used in this section of the study: (1) with the mangrove effect, as described in Section 3 settings and (2) without the mangrove effect, in which the mangrove zone (Fig. 1) is removed and Manning's coefficients inside the mangrove zone are reset to be a constant value 0.02, the same as open water areas. All of the synthetic hurricane cases are run twice using the CEST model, one with the mangrove effects and the other without the mangrove effects.

5.3. Model results

5.3.1. Sensitivity to hurricane forward speed

Firstly, we examine the sensitivity of effects of mangroves on flooding and storm surge attenuation to hurricane forward speed.

Table 2-1
Sensitivity experiments for Category 3 (Cat=3) hurricane.

Experiment #	A1	A2	A3	A4	A5	A6
Moving Speed (Mov) (m/s	2.2	2.2	6.7	6.7	11.2	11.2
Radius of maximum wind (Rmax) (km)	32	56	32	56	32	56

Table 2-2
Sensitivity experiments for Category 4 (Cat=4) hurricane.

Experiment #	B1	B2	B3	B4	B5	B6
Moving Speed (Mov) (m/s)	2.2	2.2	6.7	6.7	11.2	11.2
Radius of maximum wind (Rmax) (km)	32	56	32	56	32	56

Table 2-3
Sensitivity experiments for Category 5 (Cat=5) hurricane.

Experiment #	C1	C2	C3	C4	C5	C6
Moving Speed (Mov) (m/s)	2.2	2.2	6.7	6.7	11.2	11.2
Radius of maximum wind (Rmax) (km)	32	56	32	56	32	56

Table 2-4
Sensitivity experiments for hurricanes with different moving directions.

Experiment #	D1	D2	D3	D4	D5	D6	D7	D8	D9
Moving direction	0°	22.5°	45°	67.5°	90°	112.5°	135°	157.5°	180°

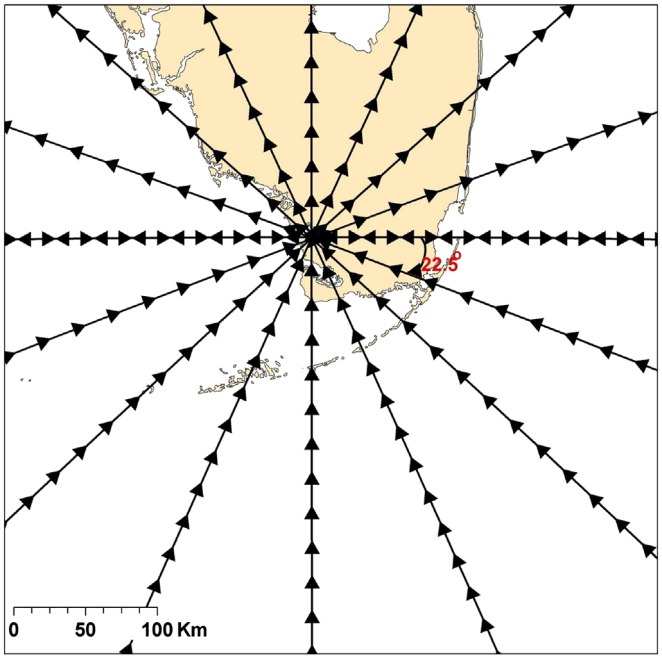

Fig. 4. The nine hurricane tracks of experiments D and the definition of hurricane approach in this study (see also Tables 2-4). 0° means the hurricane was moving from east to west, 90° from south to north and 180° from west to east.

To study flooding sensitivity to hurricane forward speed, we could compare the results of hurricanes A1, A3 and A5, or A2, A4 and A6, or B1, B3 and B5, or B2, B4 and B6, C1, C3 and C5, or C2, C4 and C6. Here only C1, C3 and C5 are discussed as an example. Fig. 5 shows the simulated maximum storm surge induced by hurricanes C1, C3 and C5. Fig. 5a, c and e shows the results of C1, C3 and C5 experiments without considering mangrove effects. The results of C1, C3 and C5 experiments considering mangrove effects are shown in Fig. 5b, d and f. Fig. 5a, c and e and Fig. 5b, d and f indicate that the flooding areas would be reduced with increasing hurricane forward speed whether or not mangroves are present, which is consistent with the other studies (e.g. Rego and Li, 2009; Peng et al., 2006). A comparison along Fig. 5a and b, Fig. 5c and d, Fig. 5e and f shows that the flooding areas were reduced obviously when mangroves were included in the model.

To quantify the sensitivity of the mangrove effect on reducing flooding areas to hurricane forward speed, the percentage of reduction in flooded areas of all hurricane cases when including mangrove effects compared to excluding mangrove effects are presented in Table 3. For example, Category 5 hurricanes with a 32 km (20 mile) radius of maximum wind speed only reduces flooded areas by 27.0% when incorporating mangrove effects if the hurricane forward speed is 2.2 m/s (5 mph); however, it would reduce the flooded areas by 30.9% if the hurricane forward speed increased to 6.7 m/s (15 mph), and the percentage reduction in flooded areas rises to 31.2% if the hurricane moves even faster (11.2 m/s or 25 mph). Other experiment results including Categories 3 and 4 hurricanes show the same trend of reduction in flooding areas as the hurricane forward speed increases (Table 3). The data in Table 3 indicate that the mangrove provides more effective protection (i.e. larger reduction in flooded area) against faster moving hurricanes than against slower moving hurricanes.

To examine the spatial difference in surge attenuation caused by the mangrove zone to hurricane forward speed, Figs. 6 and 7 show the maximum storm surge along two profile lines (indicated in Fig. 1) passing through the mangrove zone, one of which is located in the left of the hurricane track (P1) and the other is located in the right of the hurricane track (P2). The length of profile P1 and profile P2 is 24 km and 44 km respectively. The first 5 km of both profile lines is located in water areas. In order to make storm surge height comparable among different hurricane cases, Figs. 6 and 7 show the normalized storm surge using the maximum storm surge along the profile line P1 and P2 respectively. Firstly, storm surge penetrates further inland in profile P2 than in profile P1 because of stronger hurricane wind to the right of the hurricane track. For example, in Category 3 hurricanes with forward speed 2.2 m/s (5 mph) and radius of maximum wind speed 32 km (20 mile) (experiment A1), storm surge reaches only 10 km

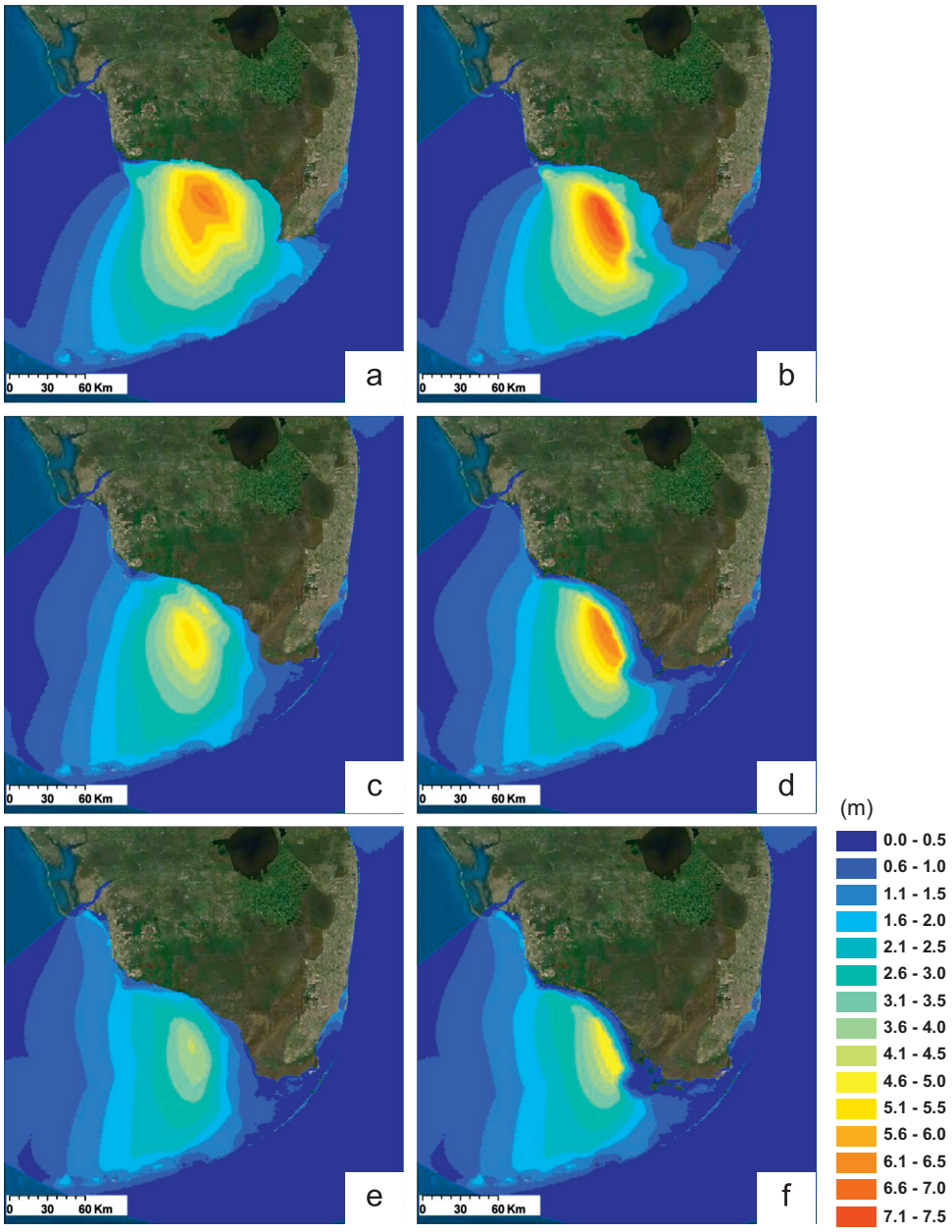

Fig. 5. The simulated maximum storm surge distribution induced by hurricanes C1, C3 and C5 without considering mangrove the zone effect (a), (c), and (e) and with considering the mangrove zone effect (b), (d), and (f) respectively.

Table 3
Percentage of reduced flooding area of sensitivity experiments (forward speed).

Forward speed (m/s)	Cat=3 ĆRmax=32	Cat=3 ĆRmax=56	Cat=4 ĆRmax=32	Cat=4 ĆRmax=56	Cat=5 ĆRmax=32	Cat=5 ĆRmax=56
2.2	30.92%	26.83%	28.26%	25.17%	26.98%	24.09%
6.7	37.85%	31.98%	33.75%	28.63%	30.93%	26.29%
11.2	42.58%	36.35%	39.79%	31.87%	37.17%	27.88%

(from 5 km to 15 km) along profile P1 (Fig. 6a); however, it propagates to 20 km (from 5 km to 25 km) along profile P2 (Fig. 7a). Figs. 6 and 7 also suggest that the mangrove zone reduces storm surge faster for fast moving hurricanes than for slow moving hurricanes in both profiles P1 and P2. No matter which category and what size of hurricanes, storm surge needs a longer distance to be attenuated to zero in slower moving hurricanes than in faster moving hurricanes. As an example, we analyze the results of experiments A1 (2.2 m/s or 5 mph), A3 (6.7 m/s or 15 mph) and A5 (11.2 m/s or 25 mph) along profile P2 (Fig. 7a), which have the same intensity (Category 3) and size (32 km or 20 mile). It needs 20 km to decay storm surge to zero from shore line point (5 km) in a slow moving hurricane (experiment A1); however, the number is decreased to 13 km and 9 km in experiments A3 and A5 when hurricane forward speed increases to 6.7 and 11.2 m/s (15 and 25 mph) respectively. This suggests that the mangrove zone plays a more effective role in protecting residents and property against fast moving hurricanes than against slow moving hurricanes.

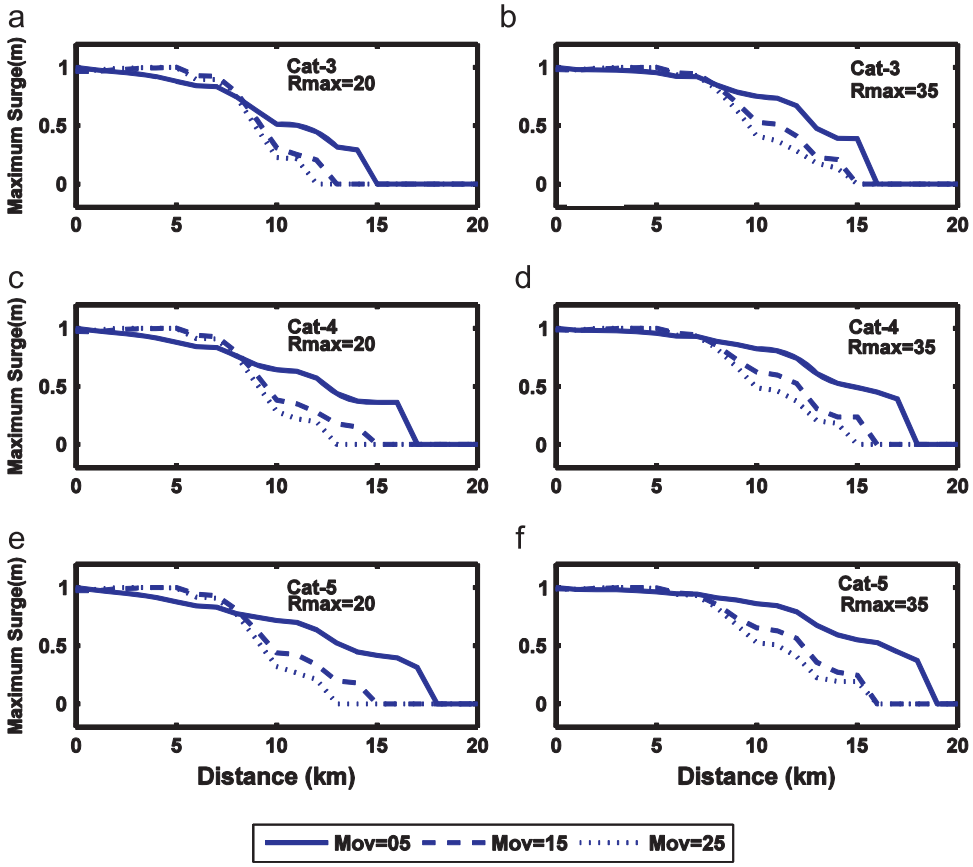

Fig. 6. Storm surge attenuation along the profile P1 passing mangrove zone of synthetic hurricanes (a) with radius maximum wind (Rmax) 32 km and Category (Cat) 3; å (b) Rmax=56 and Cat=3; (c) Rmax=32 and Cat=4; (d) Rmax=56 and Cat=4; (e) Rmax=32 and Cat=5 and (f) Rmax=56 and Cat=5. Solid line represents the synthetic hurricanes with Moving Speed (Mov) 2.2 m/s, dashed line represents Mov=6.7 m/s and dotted line represents Mov=11.2 m/s. The surge heights have been normalized to allow comparison between them, with the maximum surge height scaled to be 1.

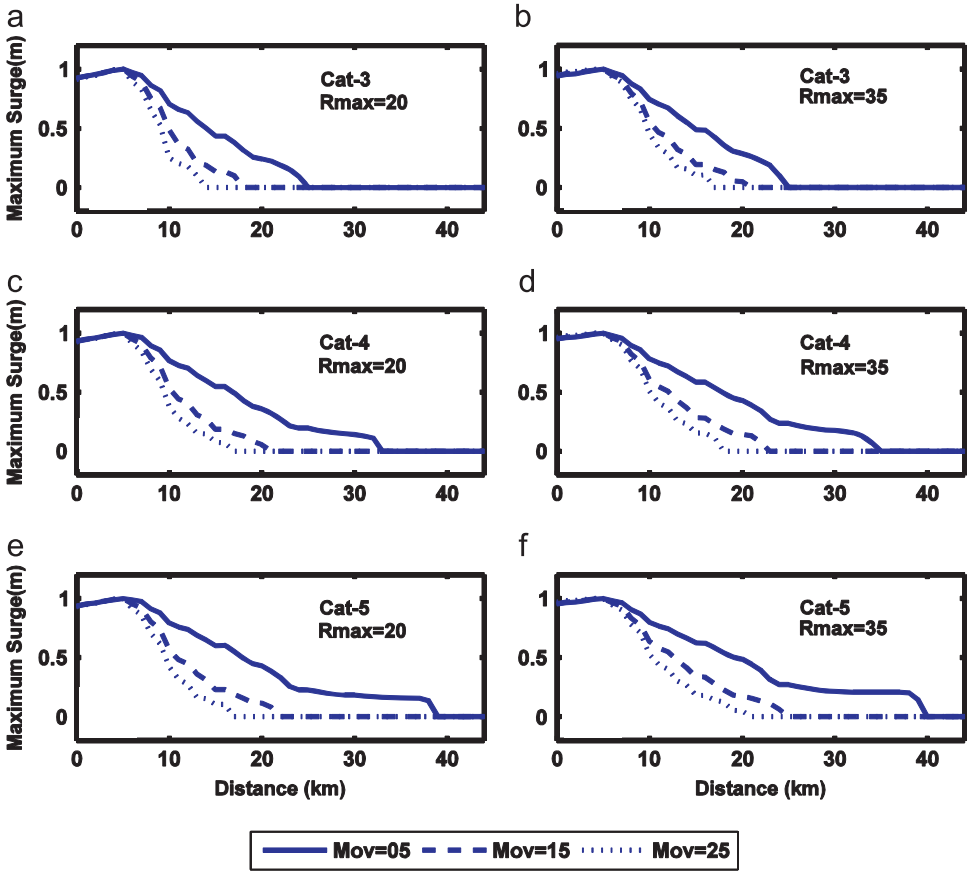

Fig. 7. Same as Fig.6 but for profile P2.

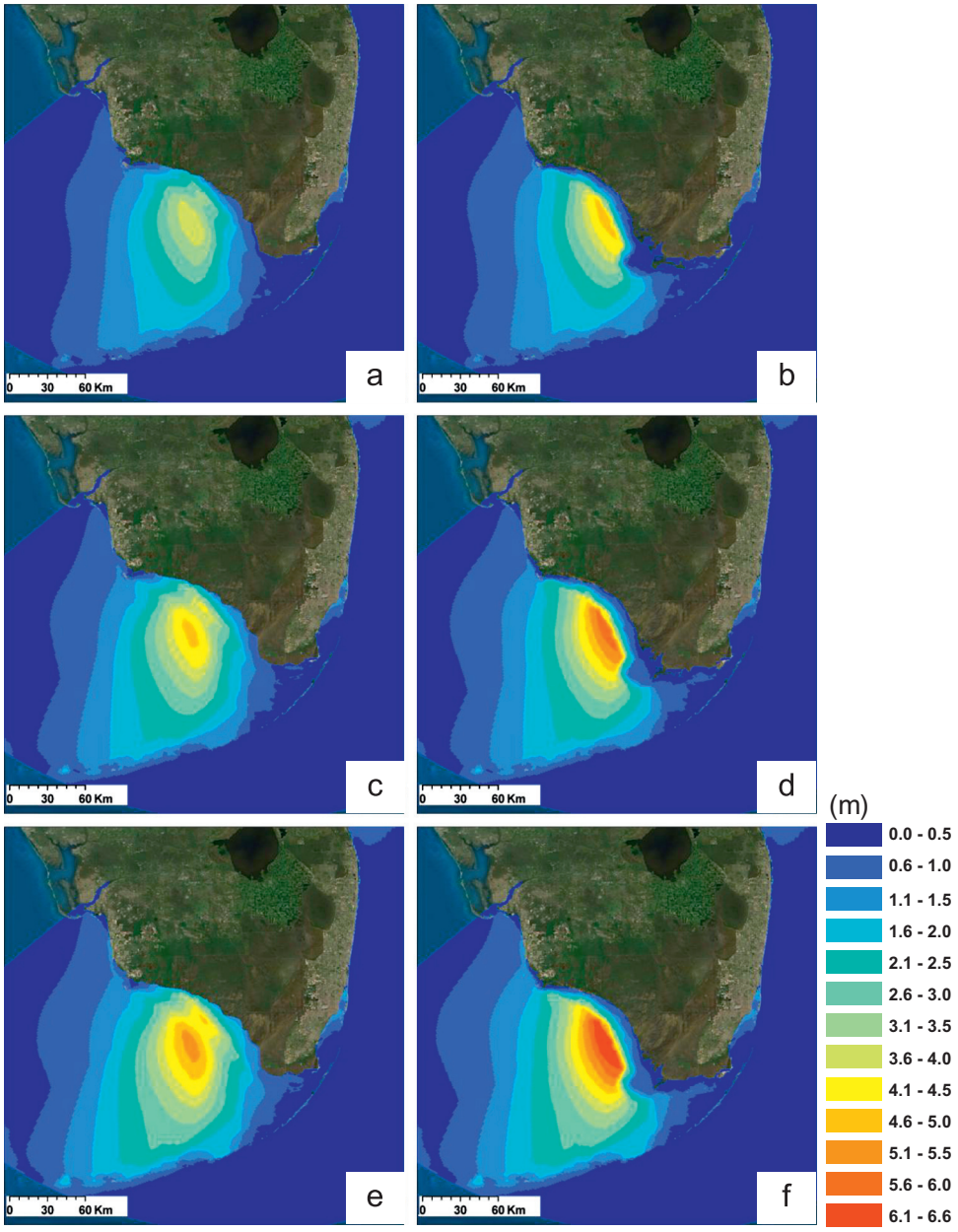

Fig. 8. The simulated maximum storm surge distribution induced by hurricanes A3, B3 and C3 without considering mangrove zone effect (a), (c), and (e) and with considering mangrove zone effect (b), (d), and (f) respectively.

Table 4
Percentage of reduced flooding area of sensitivity experiments (intensity).

Hurricane Category	Mov=2.2 ĆRmax=32	Mov=2.2 ĆRmax=56	Mov=6.7 ĆRmax=32	Mov=6.7 ĆRmax=56	Mov=11.2 ĆRmax=32	Mov=11.2 ĆRmax=56
3	30.92%	26.83%	37.85%	31.98%	42.58%	36.35%
4	28.26%	25.17%	33.75%	28.63%	39.79%	31.87%
5	26.98%	24.09%	30.93%	26.29%	37.17%	27.88%

5.3.2. Sensitivity to hurricane intensity

Secondly, the sensitivity of effects of mangroves on storm surge and flooding to hurricane intensity is studied in this section. The results of experiments A1, B1 and C1, or A2, B2 and C2, or A3, B3 and C3, or A4, B4 and C4, A5, or B5 and C5, or A6, B6 and C6 could be used as an example to investigate such sensitivity. As an example, Fig. 8 shows the simulated maximum storm surge of synthetic hurricane A3, B3 and C3. Similar to Fig. 5, Fig. 8a, c and e shows the results of A3, B3 and C3 experiments without considering mangrove effects. The results of experiments A3, B3 and C3 considering mangrove effects are shown in Fig. 8b, d and f. It shows that flooding areas reduce relatively smaller in hurricane C3 (Category 5) than in hurricane B3 (Category 4) and A3 (Category 3). Same as the analysis of sensitivity to hurricane forward speed, the exact percentages of reducing flooding areas of all hurricane cases when considering mangrove impacts are presented in Table 4. It indicates

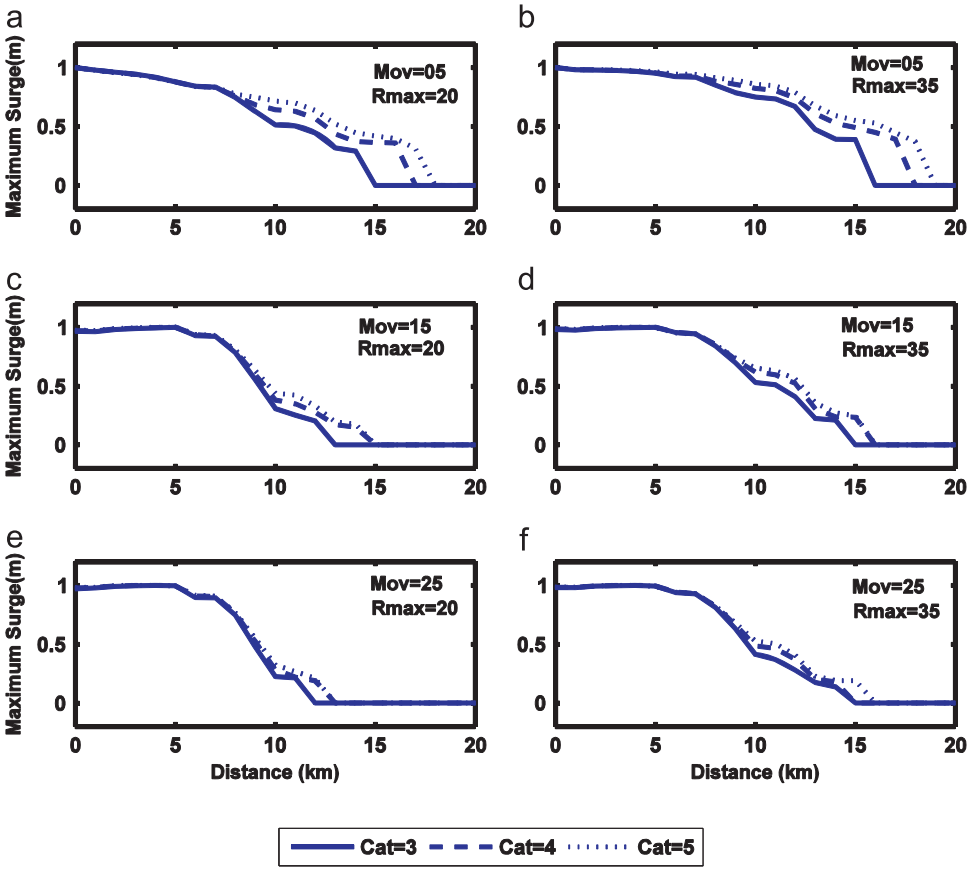

Fig. 9. Storm surge attenuation along the profile P1 passing mangrove zone of synthetic hurricanes (a) with Mov=2.2 m/s and Rmax=32 km; (b) Mov=2.2 and Rmax=56; å (c) Mov=6.7 and Rmax=32; (d) Mov=6.7 and Rmax=56; (e) Mov=11.2 and Rmax=32 and (f) Mov=11.2 and Rmax=56. Solid line represents the synthetic hurricanes with Cat=3, dashed line represents Cat=4 and dotted line represents Cat=5. The surge heights have been normalized to allow comparison between them, with the maximum surge height scaled to be 1.

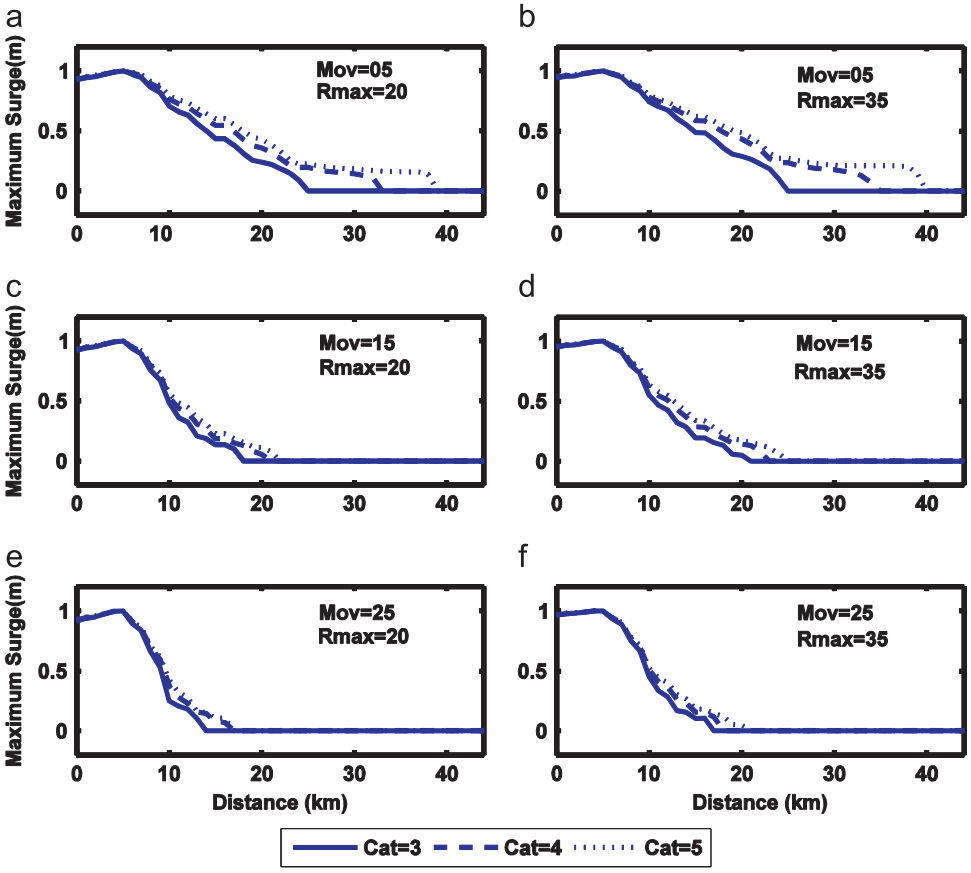

Fig. 10. Same as Fig. 9 but for profile P2.

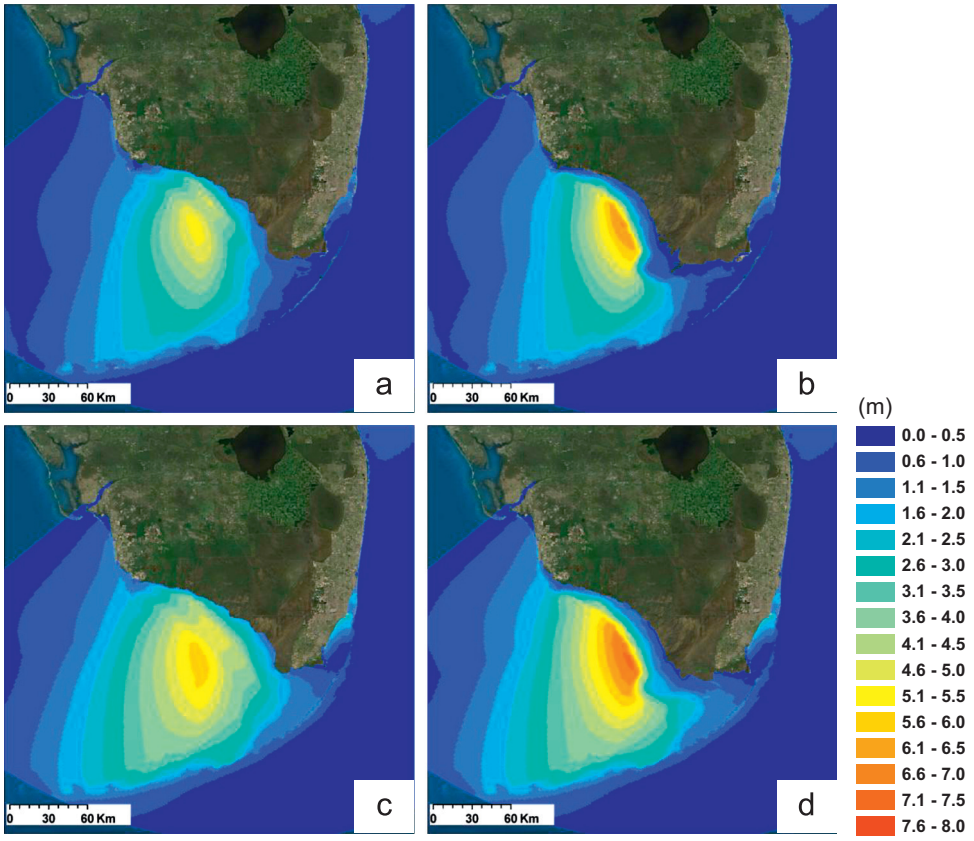

Fig. 11. The simulated maximum storm surge distribution induced by hurricanes C3, and C4 without considering mangrove zone effect (a) and (c) and with considering mangrove zone effect (b) and (d) respectively.

Table 5
Percentage of reduced flooding area of sensitivity experiments (size).

Radius of maximum wind	Cat=3 Mov=2.2	Cat=3 Mov=6.7	Cat=3 Mov=11.2	Cat=4 Mov=2.2	Cat=4 Mov=6.7	Cat=4 Mov=11.2	Cat=5 Mov=2.2	Cat=5 Mov=6.7	Cat=5 Mov=11.2
32 km	30.92%	37.85%	42.58%	28.26%	33.75%	39.79%	26.98%	30.93%	37.17%
56 km	26.83%	31.98%	36.35%	25.17%	28.63%	31.87%	24.09%	26.29%	27.88%

that the reduction in flooding areas is decreased with increasing hurricane intensity. For example, Category 5 hurricane with radius of maximum wind speed 32 km (20 mile) and moving speed 6.2 m/s (15 mph) only reduces 30.9% flooding areas if incorporating mangrove effects; however, it could reduce 33.8% flooding areas if the hurricane decreased to Category 4, and the reducing areas percentage rises to 37.9% if the hurricane decreases to Category 3 with the same size and forward speed.

The attenuations of maximum storm surge along the two profiles P1 and P2 passing the mangrove zone in all synthetic hurricane cases are shown in Figs. 9 and 10 respectively. They show that the mangrove zone reduces storm surge faster against low intensity hurricanes than against high intensity hurricanes in both profiles P1 and P2. This time the results of experiments A1 (Category 3), B1 (Category 4) and C1 (Category 5) along profile P2 (Fig. 10a) are analyzed, which have the same forward speed (2.24 m/s or 5 mph) and size (32 km or 20 mile). It needs 20 km to decay storm surge to zero from the shore line point (5 km) in a weak hurricane (experiment A1); however, the number is rising to 28 km and 34 km in experiments B1 and C1 when hurricane intensity grows to Categories 4 and 5 respectively. These results suggest that the role of the mangrove zone in protecting residents and property could be weakened against storm surge from stronger hurricanes, and might even lose its protection role against extremely strong hurricanes (e.g. mangrove zone could not be able to completely attenuate storm surge).

5.3.3. *Sensitivity to hurricane size*

Next, we examine the sensitivity of effects of mangroves on storm surge and flooding to hurricane size (radius of maximum wind speed). In this section, the results of experiments A1 and A2, A3 and A4, A5 and A6, B1 and B2, B3 and B4, B5 and B6, C1 and C2, C3 and C4, C5 and C6 could be used to show the sensitivity of mangrove protection to hurricane size. As an example, the analyses of results of hurricanes C3 and C4 are shown in Fig. 11. Similar to Fig. 5, Fig. 11a and c shows the results of C3 and C4 experiments without considering mangrove effects. The results of C3 and C4 experiments considering mangrove effects are shown in Fig. 11b and d. The reduction of the flooding area decreases against large size hurricanes, but the reduction is not as obvious as the cases shown in Figs. 5 and 8. To further examine this reduction trend, Table 5 presents percentages of reducing flooding areas of all hurricane cases when considering mangrove effects. It shows that the reduction in flooding areas by mangrove decreases with increasing hurricane sizes. For example, in Category 3 hurricane

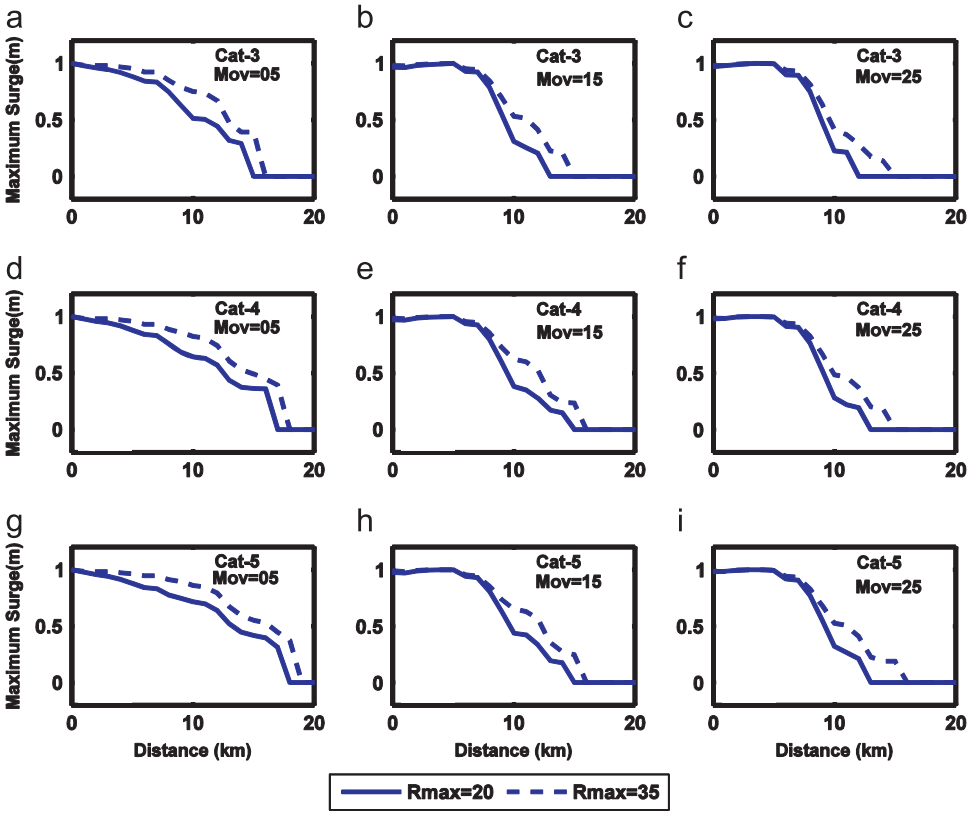

Fig. 12. Storm surge attenuation along the profile P1 passing mangrove zone of synthetic hurricanes (a) with Mov=2.2 m/s and Cat=3; (b) Mov=6.7 and Cat=3; å (c) Mov=11.2 and Cat=3; (d) Mov=2.2 and Cat=4; (e) Mov=6.7 and Cat=4; (f) Mov=11.2 and Cat=4; (d) Mov=2.2 and Cat=5; (e) Mov=6.7 and Cat=5; (f) Mov=11.2 and Cat=5. Solid line represents the synthetici hurricanes with Rmax=32 and dashed line represents Rmax=56. The surge heights have been normalized to allow comparison between them, with the maximum surge height scaled to be 1.

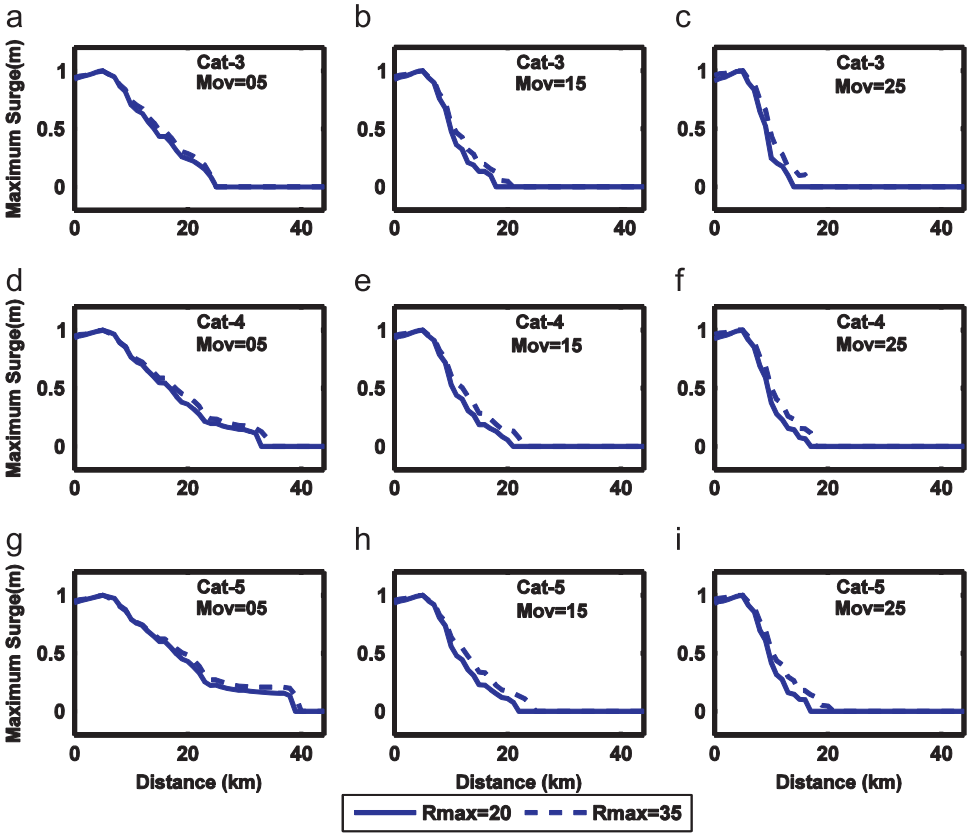

Fig. 13. Same as Fig. 10 but for profile P2.

with 6.7 m/s (15 mph) moving speed and 32 km (20 mile) of maximum wind speed radius, the reduced flooding areas are 37.9%. Meanwhile, the flooding areas are only reduced by 32.0% when the hurricane size increases to 56 km (35 mile) (maximum wind speed radius).

Figs. 12 and 13 show the attenuations of maximum storm surge along the two profiles P1 and P2 passing the mangrove zone for all synthetic hurricanes. They indicate that the mangrove zone reduces storm surge from smaller size hurricanes more effectively than those from large size hurricanes along both profiles P1 and P2. As an example, the results of experiments A3 (radius of maximum wind speed 32 km or 20 mile) and A4 (radius of maximum wind speed 56 km or 35 mile) along profile P1 are examined, which have the same forward speed (6.7 m/s or 15 mph) and intensity (Category 3). It needs 10 km mangrove to decay storm surge to zero from the shoreline (5 km) in a weak hurricane (experiment A3); however, the distance is reduced to 8 km in experiments A4 when the hurricane size grows from 32 to 56 km (20–35 mile) (Fig. 12b). Therefore, the role of the mangrove zone in protecting residents and property from storm surge impacts could be weakened for larger size hurricanes.

5.3.4. Sensitivity to hurricane moving direction

The impact of hurricane moving direction (hurricane approach angle) on hurricane-induced storm surge and coastal flooding has been recognized as an important factor (e.g. Peng et al., 2004; Rego and Li, 2009; Zhong et al., 2010). They found that the hurricane moving direction affected the flooding areas to a large extent even though other parameters remained the same. Thus, it is necessary to investigate its effect on mangrove reduction of storm surge.

The results of experiments D are analyzed to examine the effect of moving direction of hurricanes on surge reduction by mangrove. Fig. 14 shows the percentage of flooding area reduced by mangrove in the nine hurricanes (from 0° to 180°). It indicates that the dependence of mangrove reduction of coastal flooding on the hurricane moving direction does not appear to be simple linear or be monotonic. Mangrove has the biggest effect in reducing coastal flooding when hurricanes make landfall with approach angle 67.5°. In this hurricane case, the reduced flooding areas percentage by mangrove is 37.7% (Table 6). In contrast, mangrove has the least effect in reducing surge flooding when hurricanes cross Florida State from west to east (180°). The reduced flooded area percentage by mangrove is only 31.3% (Table 6). Overall, mangroves are relatively more effective of reducing storm surge flooding when hurricanes approach the west coast of South Florida with angles less than or equal to 90°, which are named here group 1 hurricanes. Meanwhile, the role of the mangrove zone in protecting residents and property from storm surge impacts could be weakened when hurricanes strike the western Florida coast with a relatively larger approach angle (larger than 90°), which are named group 2 hurricanes. Fig. 4 shows that hurricanes with an approach angle of less than 90° (group 1) travel from east to west, and on the other hand hurricanes travel from west to east if approach angle is larger than 90° (group 2). In other words, hurricanes in group 1 travel more distance over land including the mangrove zone than hurricanes in group 2 before they reach the same location. Therefore, the mangrove zone has more time to interact with hurricanes to help reduce flooding in group 1 than in group 2.

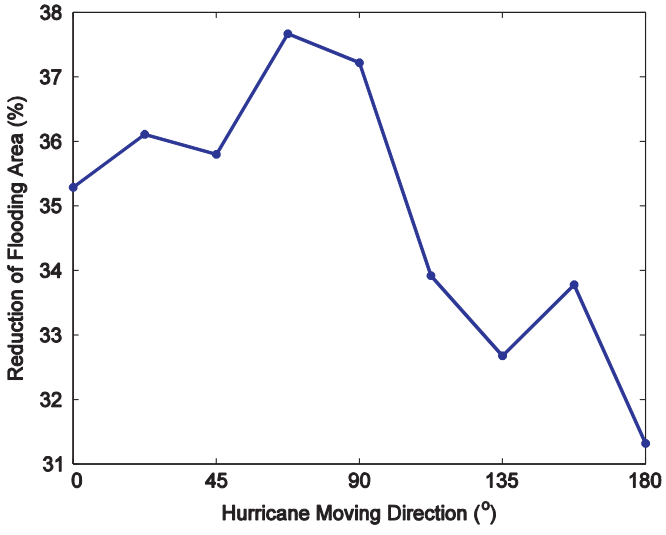

Fig. 14. Flooded area reduction as a function of hurricane approach angle.

6. Discussion

The mangrove zone plays an important role in protecting our lives and property through attenuating storm surge when hurricanes strike coastal areas. Therefore, it is crucial to quantify the reduction rate of maximum storm surge and flooded areas by mangroves to estimate the ecological service provided by mangroves. Krauss et al. (2009) suggested the reduction rates of peak water levels by the wetlands along the Gulf coast range from 4.2 to 18.9 cm/km based on field observations for hurricanes Wilma and Charley. However, the sparse field observations are not suitable for sensitivity analysis because the observations cannot capture a complete spatial pattern of mangrove effects on reducing storm surge. Furthermore, the deployment of a large amount of sensors for recording storm surge in the mangrove forest is expensive and logistically difficult. Even if a large number of observations are collected, it is almost impossible to exclude other factors from mangrove effects that may affect storm surge changes. The numerical surge model calibrated using an appropriate amount of field measurements is more efficient for such an analysis and should be recommended for quantifying the mangrove effect on attenuating storm surge.

The numerical experiments indicate that the reduction of storm surge by mangroves changes with the intensity, size, approach direction, and moving speed of a hurricane. A comparison of reduction effects among individual variables shows that the effect of the mangrove zone in reducing flooding areas and peak storm surge heights is most sensitive to the variation of hurricane forward speeds. The results of experiments A1, A3, B3 and C3 showed that the flooding reduced percentage induced by the mangrove zone in experiment A3 is 37.9% (Fig. 15), while the reduced flooding percentages decreased to 33.8% and 30.9% if the hurricane intensity was increased to Categories 4 (B3) and 5 (C3) respectively. However, if hurricane moving speed slowed from 6.7 m/s to 2.2 m/s (15 mph to 5 mph) (A1), the reduced

Table 6
Percentage of reduced flooding area of sensitivity experiments (moving direction).

Group number	1	1	1	1	1	2	2	2	2
Moving direction	0°	22.5°	45°	67.5°	90°	112.5°	135°	157.5°	180°
Reduced (%)	35.29	36.11	35.80	37.67	37.22	33.92	32.68	33.78	31.32

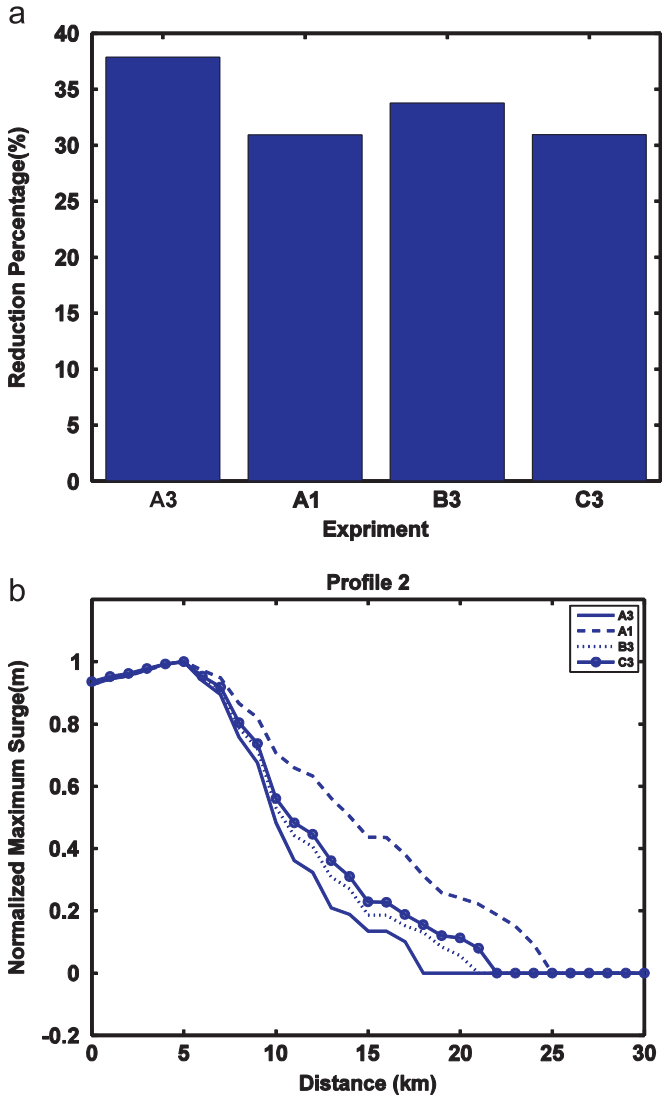

Fig. 15. (a) The reduction (in percentage) of the flooded areas by mangroves for hurricanes A1, A3, B3 and C3, and (b) storm surge attenuation along the profile P2 passing through mangrove zone of hurricanes A1, A3, B3 and C3.

flooding percentage decreased to 30.9%, which had an equivalent impact to experiment C3 (intensified 2 scales from Category 3 to Category 5). A similar conclusion can be drawn by analyzing the storm surge attenuation along the profile P2 of experiments A1, A3, B3 and C3 (Fig. 15 b). It indicated that 13 km distance was needed to decay the storm surge completely by the mangrove zone in experiment A3. If hurricane intensity upgraded to Categories 4 (B3) and 5 (C3), the distances rose to 16 and 17 km respectively. Meanwhile, the mangrove zone needed 20 km to decay the surge completely in experiment A1, even longer than in experiment C3. It demonstrated that the 67.2% variation of a hurricane forward speed may account for impacts on the mangrove protection equivalent to an upgrade or downgrade of about 2 Category hurricane intensity scales.

7. Summary and conclusion

In this study, the mangrove effects were incorporated into the storm surge model by adjusting Manning's coefficients for bottom friction according to land cover data. The numerical results of Hurricane Wilma indicate that the incorporation of the drag force from mangrove into the bottom friction item by modifying Manning's coefficients for various types of land cover is an effective way to produce the approximation of the mangrove effect on storm surge and flooding. Such validated numerical models provide a better way to analyze the sensitivity of mangrove induced reduction in storm surge height and flooded areas to hurricane characteristics by using a series of synthetic hurricanes.

Sensitivity numerical experiments indicate that the potential role of mangroves in reducing storm surge and flooding depends on the characteristics of the hurricane, such as moving forward speed, intensity, storm size and moving direction. The results suggest that mangroves are more effective at reducing the water levels and inundation of fast moving, small and weak hurricanes than those of slow moving, large and strong hurricanes. Also, it indicates that mangroves play a more effective role in reducing storm surge height and flooding areas of hurricanes moving from east to west than those of hurricanes moving from west to east in the west coast of South Florida. Overall, the mangrove reduction effect is most sensitive to the change of the hurricane forward speed.

Acknowledgments

We are grateful for proofreading by Sofia Montalvo and useful comments from two anonymous reviewers. We thank Jamie Rhome at the National Hurricane Center for providing the synthetic hurricane data set. This study is supported by a NOAA Grant NA09NWS4680018.

References

Blumberg, A., Kantha, L., 1983. Open boundary condition for circulation models. Journal of Hydraulic Engineering 112, 237–255.
Chen, C., Liu, H., Beardsley, R.C., 2003. An unstructured, finite-volume, three-dimensional, primitive equation ocean model: application to coastal ocean and estuaries. Journal of Atmospheric and Oceanic Technology 20, 159–186.
He, R., Weisberg, R., 2002. Tides on the west Florida shelf. Journal of Physical Oceanography 32, 3455–3473.
Homer, C., Huang, C., Yang, L., Wylle, B., Coan, M., 2004. Development of a 2001 national land-cover database for the United States. Photogrammetry and Remote Sensing 70, 829–840.
Jelesnianski, C.P., Chen, J., Shaffer, W.A., 1992. SLOSH: Sea, Lake and Overland Surges from Hurricanes. National Oceanic and Atmospheric Administration, Washington, DC.
Krauss, K., Doyle, T., Doyle, T., Swarzenski, C., From, A., Day, R., Conner, W., 2009. Water 666 level observations in mangrove swamps during two hurricanes in Florida. Wetlands 29, 142–149.
Large, W.G., Pond, S., 1981. Open ocean momentum flux measurements in moderate to strong winds. Journal of Physical Oceanography 11, 324–481.
Liu, H., Xie, L., 2009. A numerical study on the effects of wave–current–surge interactions on the height and propagation of sea surface waves in Charleston Harbor during Hurricane Hugo 1989. Continental Shelf Research 29, 1454–1463, http://dx.doi.org/10.1016/j.csr.2009.03.013.
Loder, N.M., Irish, J.L., Cialone, M.A., Wamsley, T.V., 2009. Sensitivity of hurricane surge to morphological parameters of coastal wetlands. Estuarine, Coastal and Shelf Science 84, 625–636.
Mattocks, C., Forbes, C., 2008. A real-time, event-triggered storm surge forecasting system for the state of North Carolina. Ocean Modelling 25, 95–119.
McIvor, A.L., Möller, I., Spencer, T., Spalding. M., 2012a. Reduction of wind and swell waves by mangroves. Natural Coastal Protection Series: Report 1. Cambridge Coastal Research Unit Working Paper 40. Published by The Nature Conservancy and Wetlands International. 27 p. ISSN: 2050-7941.
McIvor, A.L., Spencer, T., Möller, I., Spalding. M., 2012b. Storm surge reduction by mangroves. Natural Coastal Protection Series: Report 2. Cambridge Coastal Research Unit Working Paper 41. Published by The Nature Conservancy and Wetlands International. 35 p. ISSN: 2050-7941.
Peng, M., Xie, L., Pietrafesa, L.J., 2004. A numerical study on hurricane-induced storm surge and inundation in the Croatan–Albemarle–Pamlico estuary system. Estuarine, Coastal and Shelf Science 59, 121–137.
Peng, M., Xie, L., Pietrafesa, L.J., 2006. A numerical study on hurricane-induced storm surge and inundation in Charleston Harbor, South Carolina. Journal of Geophysical Research 111, C08017, http://dx.doi.org/10.1029/2004JC002755.
Rego, J.L., Li, C., 2010. Nonlinear terms in storm surge predictions: Effect of tide and shelf geometry with case study from Hurricane Rita. Journal of Geophysical Research 115, C06020, http://dx.doi.org/10.1029/2009JC005285.
Rego, J.L., Li, C., 2009. On the importance of the forward speed of hurricanes in storm surgeforecasting: a numerical study. Geophysical Research Letters 36, L07609, http://dx.doi.org/10.1029/2008GL036953.

Resio, D.T., Westerink, J.J., 2008. Modeling the physics of storm surges. Physics Today 61 (9), 33–38.
Sheng, Y.P., Lapetina, A., Ma, G., 2012. The reduction of storm surge by vegetation canopies: three-dimensional simulations. Geophysical Research Letters 39, L20601, http://dx.doi.org/10.1029/2012GL053577.
Wamsley, T.V., Cialone, M.A., Smith, J.M., 2009. Influence of landscape restoration and degradation on storm surge and waves in southern Louisiana. Natural Hazards 51, 207–224.
Wamsley, T.V., Cialone, M.A., Smith, J.M., Atkinson, J.H., Rosati, J.D., 2010. The potential of wetlands in reducing storm surge. Oceanic Engineering 37, 59–68.
Weisberg, R.H., Zheng, L.Y., 2006. Hurricane storm surge simulations for Tampa Bay. Estuaries and Coast 29 (6A), 899–913.
Westerink, J., Luettich, R.A., Baptista, A., Scheffner, N., Farrar, P., 1992. Tide and storm surge predictions using finite element model. ASCE Journal of Hydraulic Engineering 118 (10), 1373–1390.
Westerink, J., Luettich, R.A., Feyen, J.C., Atkinson, J.H., Dawson, C., Roberts, H.J., Powell, M.D., Dunion, J.P., Kubatko, ElJ., Pourtaheri, H., 2008. A basin- to channel-scale unstructured grid hurricane storm surge model applied to southern Louisiana. Monthly Weather Review 136, 833–864.
Xie, L., Liu, H., Peng, M., 2008. The effect of wave–current interactions on the storm surge and inundation in Charleston Harbor during Hurricane Hugo 1989. Ocean Modelling 20 (3), 252–269.
Xu, H., Zhang, K., Shen, J., Li, Y., 2010. Storm surge simulation along the U.S. East and Gulf720 Coasts using a multi-scale numerical model approach. Ocean Dynamics 60, 1597–1619.
Yanagisawa, H., Koshimura, S., Miyagi, T., Imamura, F., 2010. Tsunami damage reduction performance of a mangrove forest in Banda Aceh, Indonesia inferred from field data and a numerical model. Journal of Geophysical Research 115, C06032, http://dx.doi.org/10.1029/2009JC005587.
Zhang, K., Xiao, C., Shen, J., 2008a. Comparison of the CEST and SLOSH models for storm surge flooding. Journal of Coastal Research 24 (2), 489–499.
Zhang, K., Simard, M., Ross, M., Rivera-Monroy, V.H., Houle, P., Ruiz, P., Twilley, R.R., Whelan, K.R.T., 2008b. Airborne laser scanning quantification of disturbances from hurricanes and lightning strikes to mangrove forests in Everglades National Park, USA. Sensors 8 (4), 2262–2292.
Zhang, K., Liu, H., Li, Y., Xu, H., Shen, J., Rhome, J., Smith III, T.J., 2012. The role of mangroves in attenuation of storm surges. Estuarine, Coastal and Shelf Science 102–103, 11–23.
Zhong, L., Li, M., Zhang, D.L., 2010. How do uncertainties in hurricane model forecasts storm surge predictions in a semi-enclosed bay? Estuarine, Coastal and Shelf Science 90, 61–72.